Highly Sensitive and Selective Electrochemical Detection of Dopamine and Uric Acid Using Sea Urchin-like Tungsten Oxide Nanostructure Modified SPCE

Merve Oğuz[a], Ahmet Aykaç[b,**] and Mustafa Şen[c,***]

[a]Department of Biomedical Engineering Graduate Program, Izmir Katip Celebi University, Izmir, Turkey.
[b]Department of Engineering Sciences, Izmir Katip Celebi University, Izmir, Turkey
[c]Department of Biomedical Engineering, Izmir Katip Celebi University, Izmir, Turkey

ARTICLE INFO

Keywords:
Sea urchin-like WO_3
Dopamine
Uric Acid
SPCE
Artificial urine

ABSTRACT

Here, screen-printed carbon electrodes (SPCEs) were modified with ultrafine and mainly monodisperse sea urchin-like tungsten oxide ($SUWO_3$) nanostructures synthesized by a simple one-pot hydrothermal method for highly sensitive and selective detection of dopamine (DA) and uric acid (UA). Sea urchin-like nanostructures were clearly observed in scanning electron microscope images and WO_3 composition was confirmed with XRD, FTIR and UV-Vis spectrophotometer. Modification SPCEs with $SUWO_3$ nanostructures via the drop-casting method clearly reduced the R_{ct} value of the electrodes, lowered the ΔEp and enhanced the DA oxidation current due to high electrocatalytic activity. As a result, $SUWO_3$/SPCEs enabled highly sensitive detection of DA (LOD: 51.4 nM and sensitivity: 127 $\mu AmM^{-1}cm^{-2}$) and UA (LOD: 253 nM and sensitivity: 55.9 $\mu AmM^{-1}cm^{-2}$) at low concentration. Lastly, $SUWO_3$/SPCEs were tested with artificial urine, in which acceptable recoveries for both molecules were obtained. Given the high selectivity, the sensor has the potential to be used for highly sensitive simultaneous detection of DA and UA in real biological samples.

1. Introduction

Dopamine (DA) and uric acid (UA) generally coexist in biological fluids and appear to have key roles in human metabolism as well as renal and central nervous systems [1]. DA is a type of neurotransmitter and involved in regulating motivation, motor execution, cognition and reward phenomena [2]. Disruption of DA metabolism has been closely associated with various conditions/diseases ranging from heart failure to Parkinson's disease [3]. Unlike DA, UA is an end product of purine metabolism and must be eliminated by the body through urinary excretion and microbial degradation in the intestinal tract [4]. Simply put, there is no enzyme in the human body that can break down uric acid and its accumulation has been associated with various diseases including diabetes, Lesch-Nyan disease, gout, high cholesterol, hyperuricemia, heart and kidney diseases [5]. Although, these molecules can be detected using various approaches including colorimetry [6], fluorescence spectroscopy [7] and high-performance liquid chromatography [8], electrochemical detection attracts great attention due to various advantages including low cost, portability, rapid analysis, easy operation and high sensitivity [9, 10, 11]. DA and UA are both electroactive species with nearly overlapping oxidation potentials and therefore selective electrochemical detection of these molecules in biological fluids is a challenge [12, 13]. Although various nanomaterials have been proposed to overcome this challenge such as polydopamine/multi-walled carbon nanotube[14], cubic Pd - reduced graphene oxide nanocomposite [15], titanate-nanotube films [1] and one-dimensional MgO nanostructures [16], there is still need to develop novel, low-cost and highly stable electrode materials for selective detection of these molecules. Nanostructured tungsten oxide (WO_3) is a promising n-type transition metal oxide with a wide band gap ranging from 2.6 to 3.7 eV depending on particle size and shape [17]. WO_3 nanostructures finds applications in various fields ranging from photocatalysis to electrochemistry due to high electroactive surface area, decent conductivity, excellent electrochromic nature, good biocompatibility, superior charge transfer ability and good chemical adaptability [18, 19]. Although significant progress has been made in improving the electrical conductivity, charge separation and redox capacity of WO_3 by forming composition, crystal structure, morphology, and composite structures with other materials, it has not been fully explored as an electrode modifier in electrochemical sensor applications [20]. Several methods have been used to synthesize WO_3 nano derivatives including sol-gel, wet chemical, microwave-assisted, precipitation, hydrothermal, etc. Among these methods, hydrothermal attracts great attention due to advantages including effective control over the morphology of particles and size, incorporation of fewer impurities in the final product, low-cost and an practical application [21].

In this study, screen-printed carbon electrodes (SPCEs) were modified with ultrafine and mainly monodisperse sea urchin-like WO_3 nanostructures ($SUWO_3$) for highly sensitive and selective detection of DA and UA. A simple one-pot hydrothermal method was used to synthesize the nanostructures and the sea urchin-like nanostructure morphology was verified with a scanning electron microscope (SEM). Modifying the surface of SPCEs with $SUWO_3$ nanostruc-

ahmet.aykac@ikcu.edu.tr (A. Aykaç); mustafa.sen@ikcu.edu.tr (M. Şen)

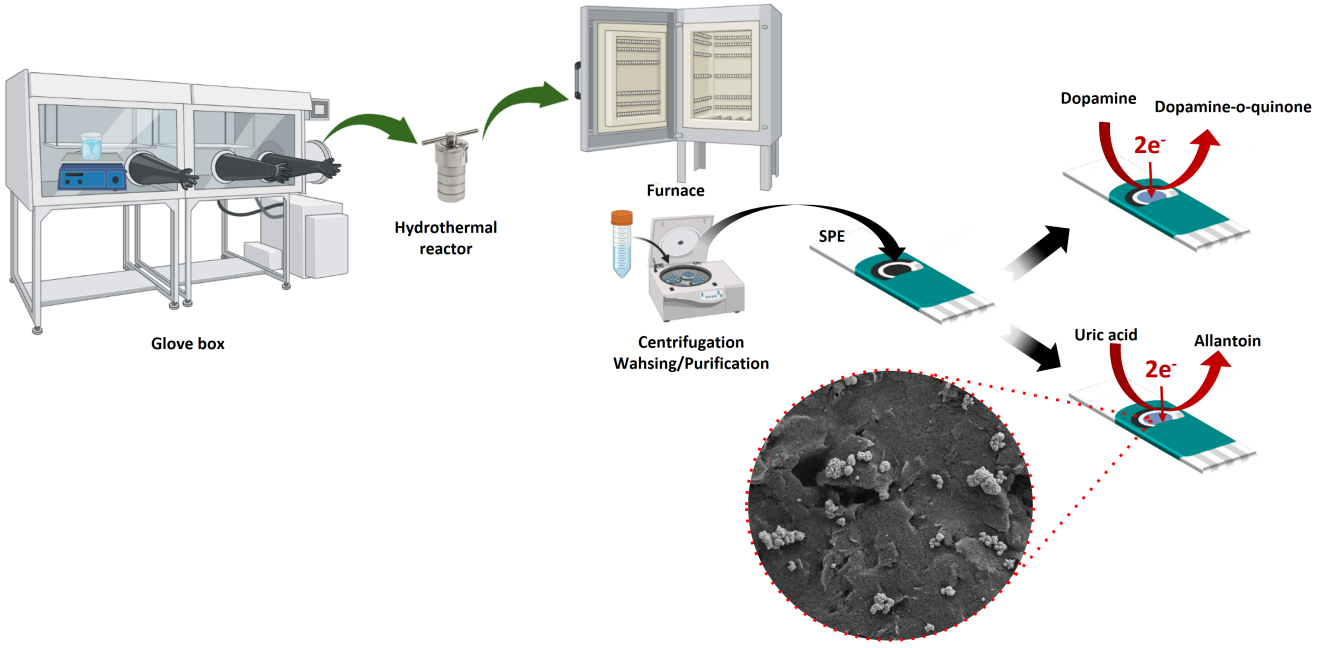

Figure 1: An illustration of the workflow adopted for the electrochemical detection of DA and UA, from hydrothermal synthesis of $SUWO_3$ nanostructures to SPCE surface modification.

tures drastically improved the electrochemical response and thus resulted in an excellent performance in detecting of DA and UA. The sensor was also tested with artificial urine, in which case acceptable recoveries for both DA and UA were obtained. To our knowledge, this is the first study to report the use of $SUWO_3$ nanostructures for highly sensitivity and selective detection of DA and UA. The sensor holds great promise to be used in real sample applications.

2. Experimental Setup

2.1. Materials

The following chemicals were purchased from Sigma-Aldrich, USA: DA hydrochloride (≥98%), uric acid (UA) (≥99%), potassium ferrocyanide ($K_4[Fe(CN)_6]$), potassium ferricyanide ($K_3[Fe(CN)_6]$), phosphate-buffered saline (PBS), urea (≥99%), calcium chloride anhydrous ($CaCl_2$) (≥97%), sodium chloride (NaCl) (≥99%), ethanol (95%). Magnesium sulfate heptahydrate ($MgSO_4.7H_2O$) (≥98%) and SPCEs were purchased from TEKKİM (Turkey) and Metroohm DropSens (Switzerland), respectively.

2.2. Synthesis of $SUWO_3$ Nanostructures

The ultrafine, mainly monodisperse $SUWO_3$ nanostructures were synthesized by a very simple and slightly modified one-pot solution-phase method [22]. Briefly, 250 mg of WCl_6 was weighed in a fume hood and added to 50 ml of pure ethanol, in which case a transparent yellow solution was rapidly formed. The resulting solution was transferred to a Teflon-lined stainless steel autoclave. Afterward, the autoclave was closed and heated in an oven at 180 °C for 24 h, then left to cool down on its own. A blue flocculent precipitate was washed with pure ethanol and dH_2O a few times to get rid of possible ions and residues. Finally, the precipitate was dried in a vacuum at 50°C with a yield of approximately 100%.

2.3. Structural Characterizations

The crystallographic structures of $SUWO_3$ was characterized using an X-ray diffraction (ARL X'TRA X-ray diffraction system, Thermo Scientific, USA) with a Cu-Kα (1.54185 Å) irradiation. Diffraction patterns in the range of 20°to 65° were recorded at 4° min^{-1} scan rate. The morphology of $WO_{2.72}$, and $SUWO_3$ modified SPCEs were examined by SEM (Carl Zeiss 300VP, SEM). The chemical composition and chemical bonds of the samples were studied by Fourier-transform infrared (FTIR) spectroscopy (Nicolet iS50 FTIR Spectrometer, Thermo Scientific, USA) in a spectral range of 4000 to 500 cm^{-1} 32 times with a resolution of 4 cm^{-1}. The absorbance of $WO_{2.72}$ nanostructures was recorded by UV-Vis (Thermo Scientific Evolution 201 UV-Visible Spectrophotometer, USA) in the region of 300 - 700 nm.

2.4. Electrochemical characterization of $SUWO_3$/SPCE

WO_3 was first dissolved in ethanol at 1 mg mL^{-1} for 5 - 6 hours in an ultrasonic bath (Elma Schmidbauer GmbH, Germany). Then, 4 µL of monodisperse $SUWO_3$ solution was drop-casted on the working electrode of an SPCE and dried at room temperature over night. All electrochemical measurements were made in a Faraday cage with using a potentiostat (Autolab PGSTAT204, Metrohm, Switzerland). Electrochemical impedance spectroscopy (EIS) mea-

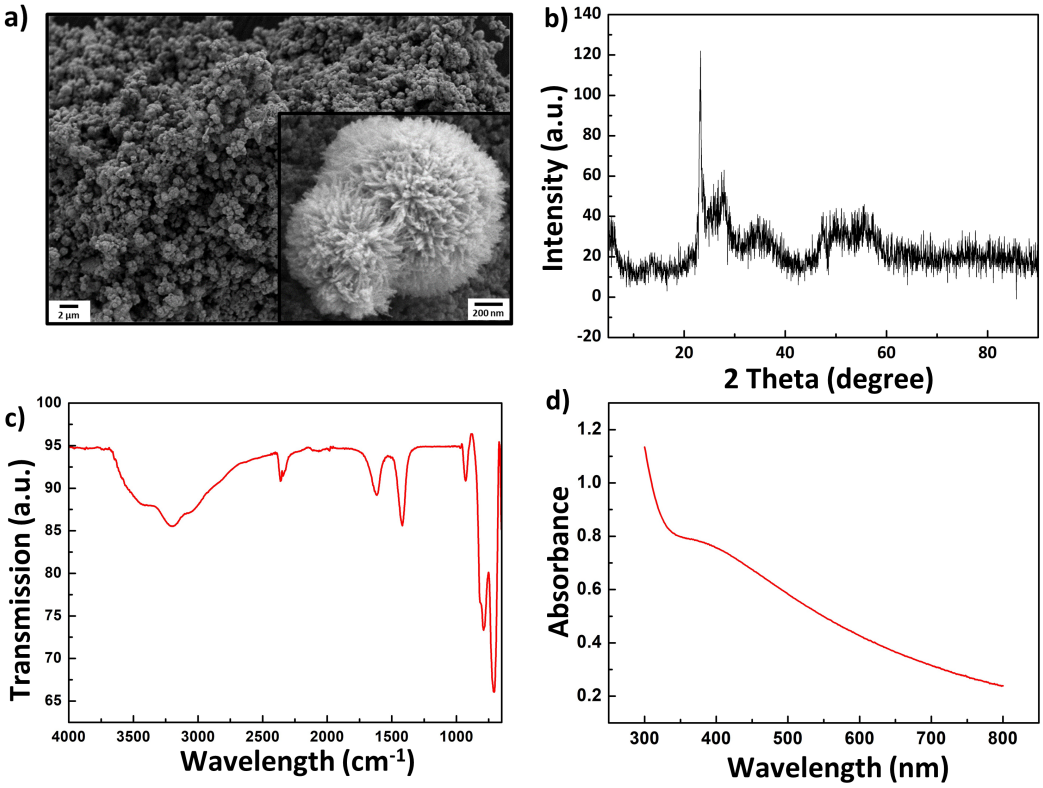

Figure 2: A SEM image (a) showing the sea urchin-like morphology of the $SUWO_3$ nanostructures along with FTIR (b), XRD (c) and UV-Vis (c) physical characterization results.

surements of bare SPCE and $SUWO_3$/SPCE were performed in a 5mM $[Fe(CN)_6]^{-3/4}$ solution containing 100 mM KCl. The impedance spectra were recorded at open circuit potential in a frequency range of 0.1 Hz to 10 kHz with a 10mV amplitude signal [23]. The R_{ct} values were obtained using the Randles circuit model through the fit and simulation program of the AUTOLAB 302 Nova 2.1.5 software.

2.5. Detection of DA and UA

Differential pulse voltammetry (DPV) technique was used for the detection of both DA and UA. Briefly, the potential of $SUWO_3$/SPCE was scanned in the ranges of 0 to 0.4 V (vs. Ag/AgCl) and 0 to 0.6 V (vs. Ag/AgCl) for the detection of DA and UA, respectively, with the following parameters; pulse amplitude: 50.55 mV, scan rate: 22 mV/s, pulse width: 50 ms. Measurements were taken in varying concentrations of DA (0, 0.1, 0.5, 1, 2.5, 5, 10, 20 and 50 µM) and UA (0, 0.1, 0.5, 1, 2.5, 5, 10, 20, 50 and 100 µM) containing PBS solutions. The maximum oxidation current values were used to draw a calibration curve and calculate limit-of-detection (LOD = $3.3*\sigma s^{-1}$) and sensitivity values for both molecules [24, 25, 26].

2.6. Selectivity and recovery tests

A selectivity test was carried out using DPV to demonstrate the selectivity of $SUWO_3$/SPCE towards DA and UA. Briefly, the electrode potential was linearly varied between -0.2 and 0.6 V (vs. Ag/AgCl) with the same parameters as described before (Section 2.5) in a PBS solution containing 50 µM DA and UA. Also, a recovery test was performed to determine the effectiveness of $SUWO_3$/SPCE in real samples. The test was carried out using DPV in an artificial urine solution containing 1.94% urea, 0.06% $CaCl_2$, 0.11% $MgSO_4.7H_2O$ and 0.80% NaCl (% w=w) [27]. Artificial urine solutions were first diluted 20-fold with PBS to contain 2.5, 5 and 10 µM DA and UA, respectively, and then used for recovery testing.

3. Results and Discussion

The synthesis of $SUWO_3$ nanostructures and preparation steps of $SUWO_3$/SPCE were depicted in Figure 1. SEM images in Figure 2a clearly confirms that the one-pot solution-phase method facilitated the successful synthesis of $SUWO_3$ nanostructures. The high surface area-to-volume ratio of the nanostructures could help drastically enhance sensitivity, especially in biosensor applications [28]. The crystalline structure of the $SUWO_3$ nanostructures was investigated by powder XRD (Figure 2b). All peaks are assigned to the monoclinic phase with the lattice parameters of a = 5.2779 Å, b = 5.1559 Å, and c = 7.6639 Å. The main diffraction peaks at 23.2°, 24.1°, 39.3°, 40.4°, and 42.2°, 49.3° are attributed to the (0 0 2), (1 1 0), (0 1 3), (2 1 1), (2 0 2), and (2 2 0) of the monoclinic phase of WO_3 (JCPDS card No. 01-088-0545). The XRD result are in line with previous reports ([29]). According to the SEM images, $SUWO_3$ nanostructures have a sea urchin-like nanostructure morphology similar to a study

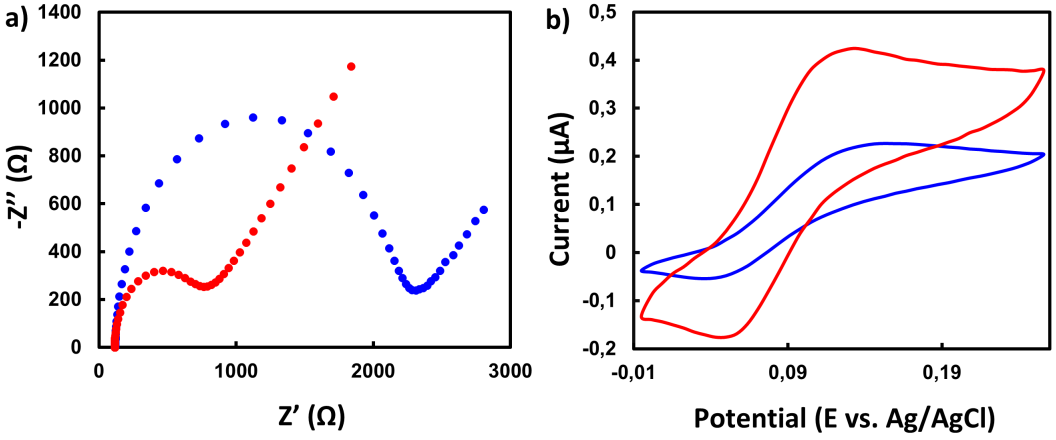

Figure 3: Nyquist (a) and CV (b) curves of bare SPCE and $SUWO_3$/SPCE demonstrating the positive influence of surface modification on the electrochemical performance. EIS and CV measurements were carried out in 5mM $[Fe(CN)_6]^{-3/4}$ and 10 µM DA, respectively.

reported by Xi et al. [22]. Basically, the nanostructures consist of a large number of radial nanowires with many nanorods around. The nanorods extending outward drastically increase the effective surface area for contact with analyte. FTIR spectra provided extra evidence for monoclinic structure of $SUWO_3$ as shown in Figure 2c. The FTIR spectra consist of three regions that are consistent with previous reports: two sharp peaks at 1401 and 1623 cm^{-1}, a broad band in the region of 3200–3700 cm^{-1} and another broad band in the region of 500–1000 cm^{-1} ([30, 31]). The sharp peaks at 1623 and 3446 cm^{-1} were assigned to the bending (H–O–H) vibration and (O–H) stretching modes, respectively. The peaks around 820 cm^{-1} correspond to W-O vibrations [32]. UV-Vis spectroscopy of the $SUWO_3$ absorbed the light at 450 nm, which matches with similar studies (Figure 2d) [33, 34].

$SUWO_3$/SPCEs were prepared by drop-casting method and electrochemically characterized to investigate the influence of surface modification on the electrochemical response. First, Nyquist curves of both bare and $SUWO_3$/SPCEs electrodes were obtained for comparison. As can be seen in Figure 3a, $SUWO_3$/SPCEs (R_{ct} = 571 Ω) displayed a lower R_{ct} value than the bare SPCE (R_{ct} = 1.99 kΩ). According to the results, it is highly likely that the nanostructures acted as "electron antennas" to enhance the electron channelling between the electrode and the electroactive species, leading to an enhanced electron transfer. Afterward, CV curves of both modified and bare SPCEs were obtained in a 10 µM DA containing PBS solution by sweeping the potential between 0 and +0.2 V (vs. Ag/AgCl) at a scan rate of 50 mVs^{-1}. As shown in Figure 3b, surface modification with $SUWO_3$ reduced ΔEp from 117 to 82 mV and resulted in a 1.67 times increase in the oxidation current, suggesting that $SUWO_3$ nanostructures have a high electrocatalytic activity for the conversion of DA. In comparison to the bare electrode, $SUWO_3$/SPCE had a better curve shape with clear anodic and cathodic peaks. In light of the EIS and CV results, one can conclude that $SUWO_3$ nanostructures can be used to effectively improve the electrochemical performance of SPCEs.

Next, the electrochemical response of $SUWO_3$/SPCE towards increasing concentrations of DA and UA was studied using DPV. Figure 4a shows the oxidation current responses of $SUWO_3$/SPCE in the range of 0.1 to 50 µM DA. The DPV curves clearly showed that $SUWO_3$/SPCE displayed a proportionally increasing current response with increasing DA concentration. The maximum oxidation currents with the corresponding DA concentrations were used to draw a calibration curve (Figure 4b). According to the results, the $SUWO_3$/SPCE displayed linear curves in the ranges of 0.1 to 50 µM and 0.1 to 2.5 µM DA with R^2 values of 0.997 and 0.999, respectively. The electrode displayed an LOD of 51.4 nM and a sensitivity of 127 $\mu AmM^{-1}cm^{-2}$. Considering the the linear range, LOD and sensitivity of $SUWO_3$/SPCE along with the physiological level of DA in nervous and bodily fluids (10 - 1000 nM) [35], it can be concluded that the sensor has the potential to be used in real sample applications. Similarly, $SUWO_3$/SPCE displayed a concentration-dependent response for UA in the range of 0.1 to 100 µM (Figure 4c). The calibration curve demonstrating the relationship between the maximum oxidation current and the UA concentration was linear in the ranges of 0.1 to 100 µM and 0.1 to 2.5 µM UA with R^2 values of 0.999 and 0.988, respectively (Figure 4d). Based on the results, the sensor had an LOD of 253 nM and a sensitivity of 55.9 $\mu AmM^{-1}cm^{-2}$. Abnormal level of UA has been associated with many life-threatening conditions including diabetes, high cholesterol and kidney disease. UA is the primary end product of purine metabolism where the enzyme xanthine oxidase breaks down xanthine to UA in the final stage. The physiological levels of UA in blood and urine is over 120-450 µM and 2 mM, respectively [5]. Considering the LOD and high sensitivity, $SUWO_3$/SPCE can be used to assess the level of UA in biological samples and thus to provide adequate feedback and treatment guidelines to patients suffering from the aforementioned conditions. A se-

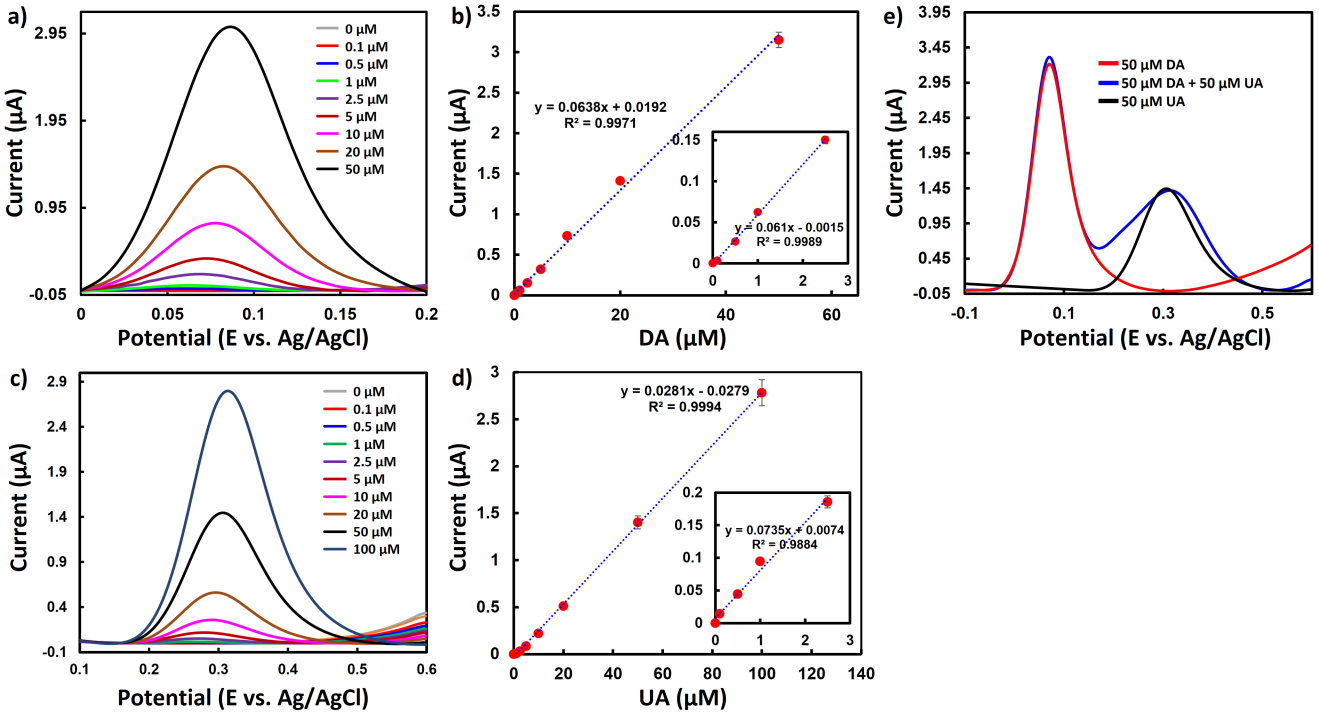

Figure 4: DPV curves of $SUWO_3$/SPCE obtained in varying concentrations of DA (a) and UA (c) along with the corresponding calibration curves (b and d). DPV voltammograms showing simultaneous and selective detection of UA and AA (d).

lectivity test was performed using three different solutions (i. 50 μM DA, ii. 50 μM DA + 50 μM UA and iii. 50 μM UA). Given the fact that the two molecules (DA and UA) are present in biological fluids and have close oxidation potentials, achieving selectivity is of great importance for real sample applications. As can be seen in Figure 4e, the current responses of DA and UA obtained in the mixture largely overlapped with individual current responses, proving that $SUWO_3$/SPCE has remarkable selectivity and can be used for simultaneous detection of these two molecules. Compared to some recently published studies, $SUWO_3$/SPCE exhibited a remarkable sensing performance in terms of both LOD and sensitivity owing to high electrocatalytic activity of the nanostructures (Table 1). Finally, known concentrations of UA and DA in artificial urine samples were used to test the recovery of $SUWO_3$/SPCE. The electrode exhibited satisfactory recoveries in detecting UA and DA, ranging from 99.6 to 105.8 % with an RSD of 2.08 to 8.71 % (Table 2). The results confirmed the accuracy and therefore the reliability of $SUWO_3$/SPCE to detect these two molecules in real samples.

Table 1
DA sensing performance of $SUWO_3$/SPCE in comparison with recent literature.

Electrode type	Analyte	Sensitivity ($\mu A m M^{-1} cm^{-2}$)	LOD (μM)	Ref.
Oxygen plasma ZnO/SPCE	DA	260	0.280	[36]
NGr-2/ITO	DA	38.8	0.131	[37]
AuNS/SPCE	DA	0.056	0.33	[38]
ZIF-67/rGO/GCE	DA	93.7	0.052	[39]
ZnO-rGO-AuNPs @SPCE	DA	-	0.294	[40]
$SUWO_3$/SPCE	DA	127	0.0514	**This work**
AuNPs/SPCE	UA	22	11.91	[41]
ND/SPCE	UA	-	0.89	[42]
Co_3O_4 NS /SPCE	UA	1560	5	[43]
GO(%10)/SPCE	UA	-	0.61	[44]
P. nigrum ZnO NPs/SPCE	UA	40.485	1.65	[45]
$SUWO_3$/SPCE	UA	55.9	0.253	**This work**

4. Conclusion

In this study, ultrafine and essentially monodisperse $SUWO_3$ nanostructures were used to improve the electrochemical performance of SPCEs for use in the detection of DA and UA. Physical characterization results proved that the simple one-pot solution-phase hydrothermal method enabled the successful synthesis of the nanostructures. The surface modification of SPCEs with $SUWO_3$ nanostructures resulted in a clearly improved electrochemical behavior as well as an increased DA oxidation current due to high electrocatalytic activity. A very low LOD and high selectivity for both DA and UA were achieved with the $SUWO_3$/SPCE sensor. Since these two molecules coexist at moderately high concentration in urine, the sensor was tested with arti-

Table 2
Detection of DA and UA in artificial urine using $SUWO_3$/SPCE.

	Added (μM)	Found (μM)	Recovery (%)	RSD (%)
DA	2.5	2.49	99.6	8.71
DA	5	4.74	94.74	5.22
DA	10	9.4	94.02	5.77
UA	2.5	2.65	105.8	6.2
UA	5	4.9	97.92	3.53
UA	10	9.4	94.03	2.08

ficial urine and acceptable recoveries were obtained for both molecules. Given its high sensitivity and selectivity, the sensor holds great promise for the simultaneous detection of DA and UA in real biological samples (e.g. urine).

Acknowledgement

This research was supported by the scientific research projects coordination unit of Izmir Katip Celebi University (project no. 2021-GAP-MÜMF-0055 and 2022-ÖDL-MÜMF-0007) and partly supported by the Scientific and Technical Research Council of Turkey (project no. 221M357).

References

[1] A. Liu, M. D. Wei, I. Honma, H. Zhou, Biosensing properties of titanatenanotube films: selective detection of dopamine in the presence of ascorbate and uric acid, Advanced Functional Materials 16 (2006) 371–376.

[2] X. Liu, L. Xie, H. Li, Electrochemical biosensor based on reduced graphene oxide and au nanoparticles entrapped in chitosan/silica sol–gel hybrid membranes for determination of dopamine and uric acid, Journal of Electroanalytical Chemistry 682 (2012) 158–163.

[3] R. Santonocito, N. Tuccitto, A. Pappalardo, G. Trusso Sfrazzetto, Smartphone-based dopamine detection by fluorescent supramolecular sensor, Molecules 27 (2022) 7503.

[4] H. Yin, N. Liu, J. Chen, The role of the intestine in the development of hyperuricemia, Frontiers in immunology (2022) 546.

[5] D. Lakshmi, M. J. Whitcombe, F. Davis, P. S. Sharma, B. B. Prasad, Electrochemical detection of uric acid in mixed and clinical samples: a review, Electroanalysis 23 (2011) 305–320.

[6] Y. Lin, C. Chen, C. Wang, F. Pu, J. Ren, X. Qu, Silver nanoprobe for sensitive and selective colorimetric detection of dopamine via robust ag–catechol interaction, Chemical Communications 47 (2011) 1181–1183.

[7] J.-L. Chen, X.-P. Yan, K. Meng, S.-F. Wang, Graphene oxide based photoinduced charge transfer label-free near-infrared fluorescent biosensor for dopamine, Analytical chemistry 83 (2011) 8787–8793.

[8] X. Hou, W. Huang, Y. Tong, M. Tian, Hollow dummy template imprinted boronate-modified polymers for extraction of norepinephrine, epinephrine and dopamine prior to quantitation by hplc, Microchimica Acta 186 (2019) 1–9.

[9] V. K. Aydin, M. Şen, A facile method for fabricating carbon fiber-based gold ultramicroelectrodes with different shapes using flame etching and electrochemical deposition, Journal of Electroanalytical Chemistry 799 (2017) 525–530.

[10] M. Şen, K. Ino, K. Y. Inoue, T. Arai, T. Nishijo, A. Suda, R. Kunikata, H. Shiku, T. Matsue, LSI-based amperometric sensor for real-time monitoring of embryoid bodies, Biosensors and Bioelectronics 48 (2013) 12–18.

[11] M. Şen, K. Ino, H. Shiku, T. Matsue, Accumulation and detection of secreted proteins from single cells for reporter gene assays using a local redox cycling-based electrochemical (lrc-ec) chip device, Lab on a Chip 12 (2012) 4328–4335.

[12] Y. Belay, A. Muller, K. Mallick, Lanthanide formate coordination polymers for selective detection of dopamine in the presence of ascorbic acid, Electrocatalysis (2022) 1–11.

[13] F. A. Bushira, S. A. Kitte, H. Li, L. Zheng, P. Wang, Y. Jin, Enzyme-like fe-n5 single atom catalyst for simultaneous electrochemical detection of dopamine and uric acid, Journal of Electroanalytical Chemistry 904 (2022) 115956.

[14] C. Wang, J. Li, K. Shi, Q. Wang, X. Zhao, Z. Xiong, X. Zou, Y. Wang, Graphene coated by polydopamine/multi-walled carbon nanotubes modified electrode for highly selective detection of dopamine and uric acid in the presence of ascorbic acid, Journal of electroanalytical Chemistry 770 (2016) 56–61.

[15] J. Wang, B. Yang, J. Zhong, B. Yan, K. Zhang, C. Zhai, Y. Shiraishi, Y. Du, P. Yang, Dopamine and uric acid electrochemical sensor based on a glassy carbon electrode modified with cubic pd and reduced graphene oxide nanocomposite, Journal of colloid and interface science 497 (2017) 172–180.

[16] M. Li, W. Guo, H. Li, W. Dai, B. Yang, Electrochemical biosensor based on one-dimensional mgo nanostructures for the simultaneous determination of ascorbic acid, dopamine, and uric acid, Sensors and Actuators B: Chemical 204 (2014) 629–636.

[17] H. Aliasghari, A. Arabi, H. Haratizadeh, A novel approach for solution combustion synthesis of tungsten oxide nanoparticles for photocatalytic and electrochromic applications, Ceramics International 46 (2020) 403–414.

[18] K. Ahmad, H. Kim, Design and fabrication of wo3/spe for dopamine sensing application, Materials Chemistry and Physics 287 (2022) 126298.

[19] D. Sandil, S. C. Sharma, N. K. Puri, Protein-functionalized wo3 nanorods–based impedimetric platform for sensitive and label-free detection of a cardiac biomarker, Journal of Materials Research 34 (2019) 1331–1340.

[20] Y. Yao, D. Sang, L. Zou, Q. Wang, C. Liu, A review on the properties and applications of wo3 nanostructure-based optical and electronic devices, Nanomaterials 11 (2021) 2136.

[21] A. Sharma, A. K. Saini, N. Kumar, N. Tejwan, T. A. Singh, V. K. Thakur, J. Das, Methods of preparation of metal-doped and hybrid tungsten oxide nanoparticles for anticancer, antibacterial, and biosensing applications, Surfaces and Interfaces 28 (2022) 101641.

[22] G. Xi, S. Ouyang, P. Li, J. Ye, Q. Ma, N. Su, H. Bai, C. Wang, Ultrathin w18o49 nanowires with diameters below 1 nm: synthesis, near-infrared absorption, photoluminescence, and photochemical reduction of carbon dioxide, Angewandte Chemie International Edition 51 (2012) 2395–2399.

[23] M. Şen, E. Azizi, İ. Avcı, A. Aykaç, K. Ensarioğlu, İ. Ok, G. F. Yavuz, F. Güneş, Screen printed carbon electrodes modified with 3d nanostructured materials for bioanalysis, Electroanalysis (2022).

[24] F. Seven, T. Gölcez, M. Şen, Nanoporous carbon-fiber microelectrodes for sensitive detection of H_2O_2 and dopamine, Journal of Electroanalytical Chemistry 864 (2020) 114104.

[25] F. Güneş, A. Aykaç, M. Erol, Ç. Erdem, H. Hano, B. Uzunbayir, M. Şen, A. Erdem, Synthesis of hierarchical hetero-composite of graphene foam/α-fe2o3 nanowires and its application on glucose biosensors, Journal of Alloys and Compounds 895 (2022) 162688.

[26] M. Sen, Using electropolymerization-based doping for the electroaddressable functionalization of a multi-electrode array probe for nucleic acid detection, Analytical Sciences 35 (2019) 565–569.

[27] J. Kim, H. Park, J. Ryu, O. Jeon, I. R. Paeng, Competitive enzyme-linked immunosorbent assay for a selective and sensitive determination of dopamine in the presence of ascorbic acid and uric acid, Journal of Immunoassay and Immunochemistry 31 (2009) 33–44.

[28] A. Aykaç, H. Gergeroglu, B. Beşli, E. Ö. Akkaş, A. Yavaş, S. Güler, F. Güneş, M. Erol, An overview on recent progress of metal oxide/graphene/cnts-based nanobiosensors, Nanoscale Research Letters 16 (2021) 1–19.

[29] Y.-C. Nah, A. Ghicov, D. Kim, P. Schmuki, Enhanced electrochromic properties of self-organized nanoporous wo3, Electrochemistry Communications 10 (2008) 1777–1780.

[30] A. Phuruangrat, D. J. Ham, S. J. Hong, S. Thongtem, J. S. Lee, Synthesis of hexagonal wo 3 nanowires by microwave-assisted hydrothermal method and their electrocatalytic activities for hydrogen evolution reaction, Journal of Materials Chemistry 20 (2010) 1683–1690.

[31] H.-F. Pang, X. Xiang, Z.-J. Li, Y.-Q. Fu, X.-T. Zu, Hydrothermal synthesis and optical properties of hexagonal tungsten oxide nanocrystals assisted by ammonium tartrate, physica status solidi (a) 209 (2012) 537–544.

[32] G. Xi, J. Ye, Q. Ma, N. Su, H. Bai, C. Wang, In situ growth of metal particles on 3d urchin-like wo3 nanostructures, Journal of the American Chemical Society 134 (2012) 6508–6511.

[33] B. Ma, E. Huang, G. Wu, W. Dai, N. Guan, L. Li, Fabrication of wo 2.72/rgo nano-composites for enhanced photocatalysis, RSC advances 7 (2017) 2606–2614.

[34] X. Guo, X. Qin, Z. Xue, C. Zhang, X. Sun, J. Hou, T. Wang, Morphology-controlled synthesis of wo 2.72 nanostructures and their photocatalytic properties, RSC advances 6 (2016) 48537–48542.

[35] X. Liu, J. Liu, Biosensors and sensors for dopamine detection, View 2 (2021) 20200102.

[36] C. Zhang, Z. Cao, G. Zhang, Y. Yan, X. Yang, J. Chang, Y. Song, Y. Jia, P. Pan, W. Mi, et al., An electrochemical sensor based on plasma-treated zinc oxide nanoflowers for the simultaneous detection of dopamine and diclofenac sodium, Microchemical Journal 158 (2020) 105237.

[37] B. J. Matsoso, B. K. Mutuma, C. Billing, K. Ranganathan, T. Lerotholi, G. Jones, N. J. Coville, The effect of n-configurations on selective detection of dopamine in the presence of uric and ascorbic acids using surfactant-free n-graphene modified ito electrodes, Electrochimica Acta 286 (2018) 29–38.

[38] I. Anshori, R. R. Althof, L. N. Rizalputri, E. Ariasena, M. Handayani, A. Pradana, M. R. Akbar, M. R. A. A. Syamsunarno, A. Purwidyantri, B. A. Prabowo, et al., Gold nanospikes formation on screen-printed carbon electrode through electrodeposition method for non-enzymatic electrochemical sensor, Metals 12 (2022) 2116.

[39] Y. Dong, J. Zheng, Tremella-like zif-67/rgo as electrode material for hydrogen peroxide and dopamine sensing applications, Sensors and Actuators B: Chemical 311 (2020) 127918.

[40] M. Gu, H. Xiao, S. Wei, Z. Chen, L. Cao, A portable and sensitive dopamine sensor based on aunps functionalized zno-rgo nanocomposites modified screen-printed electrode, Journal of Electroanalytical Chemistry 908 (2022) 116117.

[41] J. Piedras, R. B. Dominguez, J. M. Gutiérrez, Determination of uric acid in artificial saliva with compact amp3291 reader and au nanoparticles modified electrode, Chemosensors 9 (2021) 73.

[42] M. Baccarin, S. J. Rowley-Neale, É. T. Cavalheiro, G. C. Smith, C. E. Banks, Nanodiamond based surface modified screen-printed electrodes for the simultaneous voltammetric determination of dopamine and uric acid, Microchimica Acta 186 (2019) 1–9.

[43] V. Nagal, M. Khan, S. Masrat, S. Alam, A. Ahmad, M. B. Alshammari, K. S. Bhat, R. Ahmad, Hexagonal cobalt oxide nanosheet-based enzymeless electrochemical uric acid sensor with improved sensitivity, New Journal of Chemistry 47 (2023) 4206–4212.

[44] S. J. Rowley-Neale, D. A. Brownson, G. Smith, C. E. Banks, Graphene oxide bulk-modified screen-printed electrodes provide beneficial electroanalytical sensing capabilities, Biosensors 10 (2020) 27.

[45] B. Ramya, P. G. Priya, Rapid phytochemical microwave-assisted synthesis of zinc oxide nano flakes with excellent electrocatalytic activity for non-enzymatic electrochemical sensing of uric acid, Journal of Materials Science: Materials in Electronics 32 (2021) 21406–21424.